# Chelation and Mobilization of Cellular Iron by Different Classes of Chelators

G. ZANNINELLI, H. GLICKSTEIN, W. BREUER, P. MILGRAM, P. BRISSOT, R. C. HIDER, A. M. KONIJN, J. LIBMAN, A. SHANZER, and Z. IOAV CABANTCHIK

*Department of Biological Chemistry, Institute of Life Sciences, Hebrew University of Jerusalem, Jerusalem, Israel 91904 (G.Z., H.G., W.B., P.M., Z.I.C.), Liver Research Unit, Institut National de la Santé et de la Recherche Medicale U-49, Pontchaillou University Hospital, 35033 Rennes, France (G.Z., P.B.), Department of Pharmacy, King's College, W8 7AH London, UK (R.C.H.), Department of Public Health, Hadassah Medical School, Jerusalem, 91120 Israel (A.M.K.), and Department of Organic Chemistry, Weizmann Institute of Science, Rehovot 76100, Israel (J.L., A.S.)*

## SUMMARY

Iron chelators belonging to three distinct chemical families were assessed in terms of their physicochemical properties and the kinetics of iron chelation in solution and in two biological systems. Several hydroxypyridinones, reversed siderophores, and desferrioxamine derivatives were selected to cover agents with different iron-binding stoichiometry and geometry and a wide range of lipophilicity, as determined by the octanol-water partition coefficients. The selection also included highly lipophilic chelators with potentially cell-cleavable ester groups that can serve as precursors of hydrophilic and membrane-impermeant chelators. Iron binding was determined by the chelator capacity for restoring the fluorescence of iron-quenched calcein (CA), a dynamic fluorescent metallosensor. The iron-scavenging properties of the chelators were assessed under three different conditions: (a) in solution, by mixing iron salts with free CA; (b) in resealed red cell ghosts, by encapsulation of CA followed by loading with iron; and (c) in human erythroleukemia K562 cells, by loading with the permeant CA-acetomethoxy ester, *in situ* formation of free CA, and binding of cytosolic labile iron. The time-dependent recovery of fluorescence in the presence of a given chelator provided a continuous measure for the capacity of the chelator to access the iron/CA-containing compartment. The resulting rate constants of fluorescence recovery indicated that chelation in solution was comparable for the members of each family of chelators, whereas chelation in either biological system was largely dictated by the lipophilicity of the free chelator. For example, desferrioxamine was among the fastest and most efficient iron scavengers in solution but was essentially ineffective in either biological system when used at $\leq 200$ $\mu M$ over a 2-hr period at 37°. On the other hand, the highly lipophilic and potentially cell-cleavable hydroxypyridinones and reversed siderophores were highly efficient in all biological systems tested. It is implied that in K562 cells, hydrolysis of these chelators is relatively slower than their ingress and binding of intracellular iron. The chelator-mediated translocation of iron from cells to medium was assessed in $^{55}Fe$-transferrin-loaded K562 cells. The speed of iron mobilization by members of the three families of chelators correlated with the lipophilicity of the free ligand or the iron-complexed chelator. The acquired information is of relevance for the design of chelators with improved biological performance.

Iron-chelation therapy is mandatory for the treatment of patients with secondary iron overload (1–6). In these patients, iron chelation prevents labile iron from engaging in radical-mediated damage of crucial organs such as the heart and liver. Only the natural siderophore chelator DFO has been approved for therapeutic use. However, this otherwise useful agent has a major drawback in that having to be administered parenterally, it poses some difficulties with patient compliance and the high cost of patient care (4, 5). It also is not devoid of side effects, which can be fatal (5). Therefore, major efforts have been invested in developing improved chelators, including oral preparations, as potentially safe substitutes for DFO, but thus far, success has been limited (6).
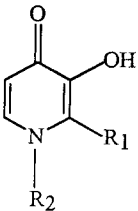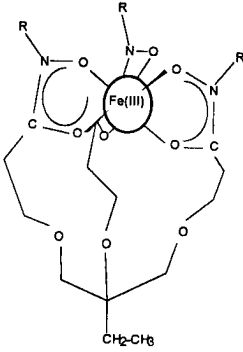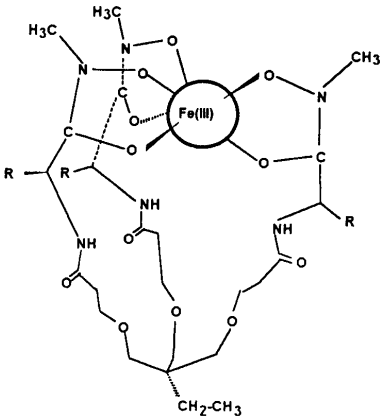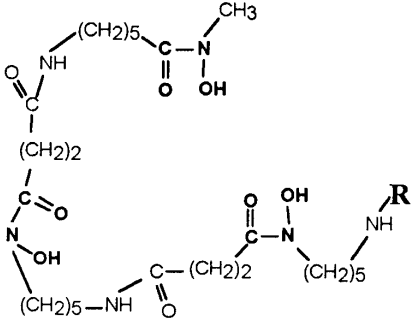
In considering the factors that contribute to the biological efficacy of iron chelators, previous studies have focused primarily on the relatively high iron-binding affinity ($pK_{IC} > 27$) for specificity and on the relatively high lipid/water PC for

---

**ABBREVIATIONS:** DFO, desferrioxamine; HPO, hydroxypyridinone; RSF, reversed siderophore; CA, calcein; CA-AM, calcein-acetomethoxy ester; Tf, transferrin; PC, partition coefficient; LIP, labile iron pool; FAS, ferrous ammonium sulfate; SIH, salicylaldehyde isonicotinoyl hydrazone; HBS, HEPES-buffered saline; HEPES, 4-(2-hydroxyethyl)-1-piperazineethanesulfonic acid; MEM, minimal essential medium; $\alpha$-MEM-HEPES; HEPES-buffered, bicarbonate-free $\alpha$-MEM containing 20 mM HEPES, pH 7.3; DMSO, dimethylsulfoxide.

TABLE 1

**Structures and partition coefficients of chelators**

| | Chelator name | Group R1 | Group R2 | PC | |
|---|---|---|---|---|---|
| | | | | Free ligand | Iron complex |
| | CP20 | $CH_3$ | $CH_3$ | 0.17 | 0.0025 |
| | CP40 | $CH_3$ | $(CH_2)_2O$ | 0.002 | 0.002 |
| | CP51 | $CH_3$ | $(CH_2)_2 OCH_3$ | 0.3 | 0.005 |
| | CP94 | $C_2H_5$ | $C_2H_5$ | 0.85 | 0.07 |
| | CP96 | $C_2H_5$ | $(CH_2)_2 OCH_3$ | 0.83 | 0.05 |
| | CP102 | $CH_2CH_3$ | $(CH_2)_2 OH$ | 0.22 | 0.0018 |
| | CP117 | $CH_2CH_3$ | $(CH_2)_2 OCOC(CH_3)_3$ | 14.4 | 102 |
| | CP41 | $CH_3$ | $(CH_2)_3 OH$ | 0.13 | 0.0012 |
| | CP165 | $CH_3$ | $(CH_2)_3 OCOC (CH_3)_3$ | 9.0 | 84.5 |

| | Chelator name | GroupR | PC |
|---|---|---|---|
| | RSFm2 | $CH_3$ | 1.7 |
| | RSFm2(H) | H | 0.12 |
| | RSFm2pa | $(CH_2)_2COOH$ | 0.13 |
| | RSFm2pee | $(CH_2)_2COOC_2H_5$ | 13.5 |

RSFm2

| | RSFm2leu | $CH_2CH(CH_3)_2$ | 12.5 |
|---|---|---|---|
| | RSFm2ileu | $CH(CH_3)CH_2CH_3$ | 14.0 |
| | RSFm2phe | $CH_2C_6H_5$ | 40 |

| | DFO | H | 0.7 |
|---|---|---|---|
| | MADFO | $COC_6H_5NHCH_3$ | 3.4 |

rapid access into intracellular compartments. High PC of the chelator/iron complex that is formed intracellularly was considered advantageous not only for rapid access into cells and removal of iron from cells *per se* but also for minimizing cell exposure to potentially toxic iron/chelator complexes. This would certainly be the case for most chelators, excluding those that fully coordinate the bound iron, such as in hexadentate complexes. Few studies have systematically assessed the physicochemical parameters that determine the efficacy of chelators as cell iron scavengers in terms of their speed and ability to chelate intracellular iron and subsequently translocate the chelated iron from cells to medium. A preliminary study has been recently conducted with a range of HPOs on isolated rat hepatocytes (7). However, the various chemical steps of chelator interaction with cells have not been kinetically determined for the major families of chelators.

In this work, we used two membrane model systems to assess three different families of iron chelators in terms of their capacity to reduce cell iron pools; these include HPOs (8) and the hydroxamate-based RSFs (9) and DFO derivatives (10). The three families differ in their iron-binding stoichiometry, geometry, and lipophilicity. The HPOs comprise bidentate binders that are likely to form iron complexes of varying metal/ligand stoichiometries and configurations (including cisoid and transoid configurations). The hydroxamate-based RSFs are tripodal ligands that form complexes of defined 1:1 metal/ligand stoichiometries and single cisoid configurations, whereas the DFOs are linear ligands that form 1:1 iron complexes of both cisoid and transoid configurations. It is yet to be determined to what extent structure uniformity might also contribute to the efficacy of the chelators in accessing cells, binding chelatable iron, and translocating it out of the cell.

Human resealed erythrocyte ghosts loaded with iron(III) were used as a simple membrane model for assessing chelator permeation and intravesicular iron(III) binding. Human erythroleukemia K562 cells were used for assessing the ability of the chelators to affect the LIP of cells and extract iron from cells into the medium. We applied here our recently developed method of continuous and *in situ* monitoring of intracellular iron with the fluorescent metallosensitive probe CA (11, 12). The fluorescence of cell-loaded CA, which is quenched by intracellular iron, can be restored by chelators at a speed and extent dictated by their membrane permeation and metal binding kinetics and affinity (12). This method provides a measure for free chelator permeation and intracellular iron binding. It was complemented with the measurement of extraction of $^{55}$Fe from Tf-$^{55}$Fe-preloaded K562 cells, which in turn provided a measure for translocation of the chelator/iron complex from cells to medium. These systematic studies enabled us to obtain an iron-scavenging profile for each class of iron chelator based on their physicochemical properties and relevance to both pharmacology and future drug design.

## Experimental Procedures

### Materials

CA and CA-AM were obtained from Molecular Probes (Eugene, OR). FAS was from Sigma Chemical (St. Louis, MO). All other materials were of the highest available grade. The following iron chelators were prepared as 50 mM stock solutions in DMSO: 3-Hydroxy-2-methyl-pyridin-4-ones were synthesized and purified as previously described (13); SIH was generously provided by Dr. P. Ponka (Lady Davis Institute for Medical Research, Montreal, Canada); DFO methylsulfonate (Ciba-Geigy, Basel, Switzerland); and the reversed siderophores RSFphe, RSFi-leu, RSFleu, RSFpee, and RSFm2, and *N*-methylanthranilic/DFO were prepared according to previously described protocols (9, 10, 13a). Chromatographically pure Tf and Apo-Tf were from Kama-Da Industries (Kibbutz Kama, Israel). The chemical formulas of agents used in this study and their octanol/saline PCs are given in Table 1.

### Effects in Solution

**Determination of chelator efficiency.** CA fluorescence [excitation, 486 nm (range, 480–490 nm); emission, 517 nm (range, 510–517 nm)] was measured in a PTI Oscar fluorescence station (PhotoMed, Wedel, Germany) equipped with a temperature-controlled cuvette holder and magnetic stirrer. Data were recorded on-line and analyzed by Origin software (Microcal) on a PC-compatible computer. Fluorescence measurements in solution were performed at room temperature using a 100 nM solution of CA (free acid) in HBS, pH 7.2 (20 mM HEPES, 150 mM NaCl). An aliquot from an aqueous FAS solution was added (1 μM final concentration) until maximal quenching was obtained and was followed by the addition of 5 μM chelator, unless indicated otherwise. After fluorescence recovery (dequenching), SIH at 100 μM (final) was added to obtain maximal dequenching. Data were normalized to the maximal fluorescence attained with SIH.

### Effects in Resealed Ghosts

**Loading of CA and iron.** CA (free acid) was incorporated into red cell ghosts by encapsulation. Briefly, 1 ml of washed human red blood cells (80% hematocrit, in HBS, pH 7.2) was added to 70 ml of hemolysis buffer (4 mM MgSO$_4$, 1.33 mM NaH$_2$PO$_4$, 8.7 mM NaCl, 0.009% acetic acid), incubated for 10 min in ice-cold water, and centrifuged (8000 × g for 5 min), and the pellet was washed again with the same hemolysis buffer and then resuspended in 4 ml of HBS, pH 7.2, containing 1 mM MgCl$_2$ and 100 μM CA (free acid) in the cold for 10 min. The suspension was transferred to 37° and incubated for 1 hr, washed extensively with HBS (5°), and resuspended in 1 ml of HBS. The ghost-entrapped CA was ~30 μM. The ghost suspension was supplemented with 100 μM FAS and incubated at room temperature (~60 min) until all (>90%) the fluorescence was quenched. The ghosts were washed in the cold, first with HBS containing 1 mM diethylenetriaminepentaacetic acid and then with HBS alone, and finally resuspended in the cold in 200 μl of HBS (ghost stock).

**Assessment of chelator action.** Ghosts (10 μl from the stock) were suspended in a cuvette containing 1 ml of HBS that was placed in the thermostated cell compartment (25°) of the fluorimeter described above. Fluorescence was followed with time. After a stable base-line was attained, the HPO or RSF was added at a 100 μM final concentration, unless stated otherwise. Traces were recorded for a given time period, and dequenching was monitored. Complete dequenching was attained by the addition of 100 μM SIH.

### Effects in Cell Cultures

**Cell treatment and loading with CA.** Human erythroleukemia K562 cells were propagated in α-MEM containing 7% fetal calf serum supplemented with L-glutamine and antibiotics (19). Cells were loaded at a density of 1–3 × 10$^6$ cells/ml with 0.125 μM CA-AM for 5 min at 37° in α-MEM-HEPES, washed of excess CA-AM, resuspended in α-MEM-HEPES, and maintained at room temperature until use. Just before measurements, 1 ml of CA-loaded cell suspension (~ 5 × 10$^6$ cells) was centrifuged in a microcentrifuge, and the cells were resuspended in 2 ml of prewarmed 150 mM NaCl, 10 mM HEPES-Tris, pH 7.3 (HBS buffer). Aliquots of the cell suspension

were transferred to each of four stirred, thermostated (37°) cuvettes that were placed in a four-cell turret. Fluorescence measurements were obtained sequentially for each cuvette and computer recorded. A fluorescence-quenching, anti-CA antibody (10 $\mu$l/cuvette) was added to eliminate all extracellular fluorescence, which amounted to ~2% of the total fluorescence. The base-line signal leakage of the probe during the experimental period was <5% leakage of CA/hr at 37°.

**Fluorescence measurements and calibration.** The concentration of free CA inside cells was found to be directly proportional to the length of incubation and CA-AM concentration. It was estimated as follows: ~$2 \times 10^7$ CA-loaded cells were centrifuged in a narrow-bore microcentrifuge, giving a packed cell volume of 20 $\mu$l. The cell pellet was solubilized in 2 ml of HBS buffer containing 1.5% octyl-glucoside and 200 $\mu$M diethylenetriaminepentaacetic acid. The CA concentration in the cell lysate was determined from its fluorescence and compared with that of CA standards in the same solution, giving an intracellular CA concentration of 10 $\mu$M.

**Assessment of chelator action.** CA-loaded cells were suspended in HBS ($1 \times 10^6$ cells/ml) with gentle stirring of the cuvette contents, and fluorescence was monitored. After a stable base-line was attained, chelator was added at different concentrations (10, 30, 50, and 100 $\mu$M final concentration), traces were recorded for a given time period, and finally SIH (100 $\mu$M) was added to attain maximal dequenching.

**Preparation of Tf-$^{55}$Fe.** $^{55}$FeCl$_3$, 0.4 mCi (Amersham, Buckinghamshire, UK) was complexed to NTA at a ratio of 0.18 $\mu$mol of Fe/1.8 $\mu$mol of NTA, followed by the addition of 0.045 $\mu$mol of apotransferrin dissolved in 0.5 M Tris·HCl/0.1 mM NaHCO$_3$, pH 8.5. Tf-$^{55}$Fe was separated from nonbound $^{55}$Fe by gel filtration on a PD-10 column preequilibrated with HBS (Pharmacia, Uppsala, Sweden).

**Loading of K562 cells with Tf-$^{55}$Fe.** A suspension of ~$5 \times 10^7$ K562 cells in 20 ml of $\alpha$-MEM-HEPES was incubated with Tf-$^{55}$Fe (final concentration 5 $\mu$g/ml) for 30 min at 37°. The cells were then washed twice, resuspended in full $\alpha$-MEM, divided into equal aliquots of ~$5 \times 10^6$ cells in 1 ml, and plated onto 24 multiwell plates. Various chelators were added at a concentration of 100 $\mu$M and incubated for 0–120 min at 37°. The cells were then centrifuged, and a sample of the supernatant was taken for determination of $^{55}$Fe release in a 3-ml scintillation cocktail (Quicksafe, Zinnser Analytic, Frankfurt, Germany).

**Effect of chelators on K562 cell nucleic acid synthesis.** Cells taken at the exponential phase of growth were placed onto 24-well plates, and treated with 10 or 50 $\mu$M chelator (added from a 50 mM stock solution in DMSO) in growth medium for 16 hr. Control cells were treated with only the aprotic solvent (0.2–0.5% final concentration). After this incubation period, the cells were either centrifuged and resuspended in fresh growth medium supplemented with $^3$H-labeled hypoxanthine (1 $\mu$Ci/ml) or $^3$H-labeled thymidine (1 $\mu$Ci/ml) and incubated for an additional 6 hr (drug exposure + wash = residual effect) or directly supplemented with the radioactive materials (continuous exposure). Incorporation of radioactivity into nucleic acid material was assessed by analyzing the samples with a cell harvester and a Beckman Liquid Scintillation Counter as we previously described (19).

## Results

The method used for assessing ingress of chelators into cells was based on chelator-evoked increase in the fluorescence of iron-quenched CA. As previously shown, CA, a fluoresceinated analog of EDTA, binds iron(II) and iron(III) with affinities similar to those of EDTA (1014 and 1024 M$^{-1}$, respectively) (7). However, due to its polynucleated nature, iron(III) reacts slowly with CA in physiological solutions. Conversely, iron(II) (0.2 $\mu$M) added to a CA solution (100 nM)

leads to a swift and full quenching of fluorescence (Fig. 1A). In the CA-bound form, iron(II) oxidizes to iron(III), and concomitantly, the stability of the iron/CA complex increases (10). Removal of iron from the CA/iron complex by different chelators is visualized as a rise in fluorescence. The speed and extent of fluorescence recovery depend on the kinetics of iron binding and the relative binding affinities, concentrations, and stoichiometries of iron binding. As shown in Fig. 1A, fluorescence was readily reversed by the addition of different hydroxypyridinones (5 $\mu$M) that vary in lipophilic character but have similar iron(III) binding affinities and a similar 3:1 iron-binding stoichiometry (7). Although at the concentration used, all the chelators eventually led to full restoration of fluorescence (not shown), we opted for rapid maximal reversal by addition of excess SIH, a fast acting iron chelator (14). This value was used for normalizing the systems. The calculated slopes of reversal represent the apparent rate constants of iron binding by the respective chelators. The values were comparable for the four chelators shown in Fig. 1A. Similar data were obtained with hydroxamate-based chelators (DFOs and RSFs) that form 1:1 iron complexes (Fig.
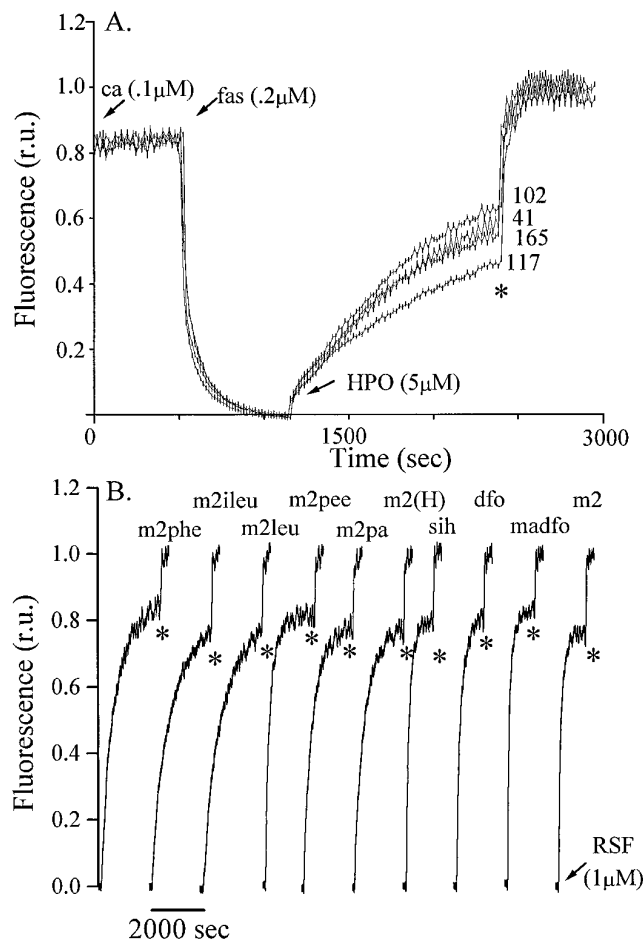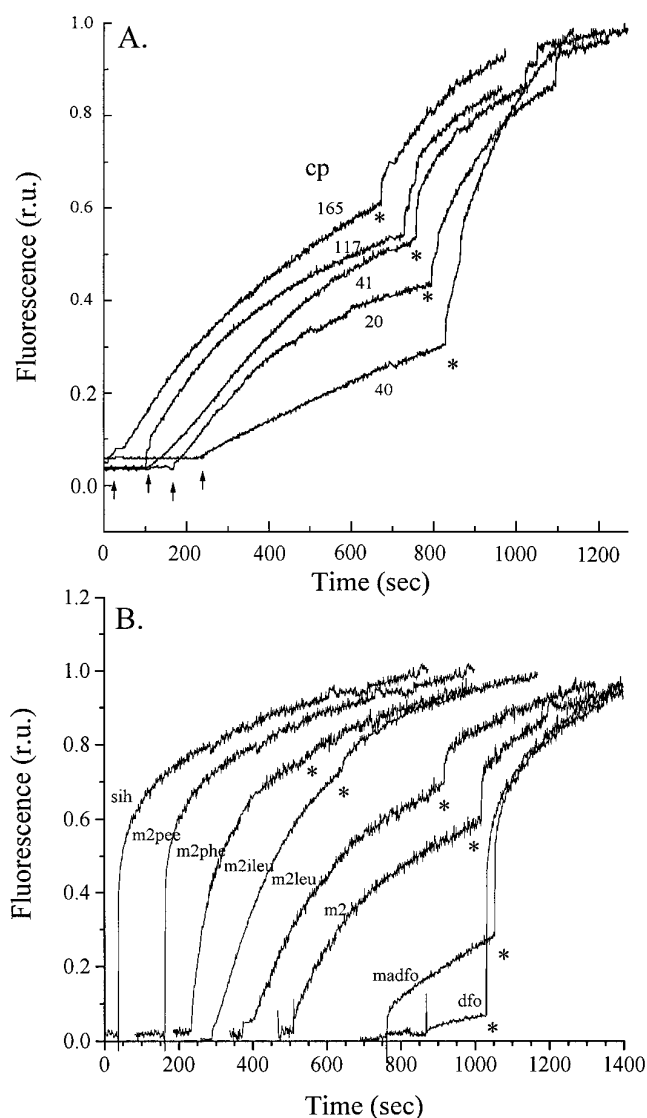


**Fig. 1.** Dequenching of CA/iron complexes by chelators in solution. CA (100 nM) was dissolved in HBS, pH 7.2, at room temperature (base-line). After 0.2 $\mu$M FAS produced 100% quenching of fluorescence, either HPO 102, at 5 $\mu$M (A), or RSFm2, at 1 $\mu$M (B), was added. *, Addition of 100 $\mu$M SIH. Data were normalized to the maximal level of fluorescence attained after the addition of SIH. *Scale*, relative fluorescence units (r.u.) against time (sec). Background fluorescence represented <3% of the maximal fluorescence signal. B, Only the part of the experiment pertinent to chelator effect is shown.

1B). In this case, however, the depicted traces represent only the fluorescence recovery phase of CA in solution after the addition of two DFOs and several RSFs that vary enormously in their hydrophilic/lipophilic balance. As with the HPO, these hexadentate agents displayed comparable speeds and extents of iron binding in solution. Small differences could be accounted for by steric constraints in the iron exchange process and iron complex formation (16).[1]

**Iron chelation in resealed ghosts.** Red cell membrane ghosts loaded with iron/CA complexes were used as a model for assessing a possible correlation between scavenging cell iron and the permeation properties of the chelators. As previously shown in this model, virtually all the CA-complexed iron is in the iron(III) form, so recovery of fluorescence is commensurate with intravesicular scavenging of iron(III) by the permeating chelator. To exclude changes in fluorescence due to chelator reaction with CA/iron(III) that might have leaked from cells, all systems contained anti-CA antibody that demonstrably bound all external CA and quenched its fluorescence (11, 12). Fig. 2A depicts the time dependence of fluorescence recovery obtained after the addition of five HPOs that were selected on the basis of structural analogy but marked differences in lipophilicity (i.e., PCs). The addition of chelator led to a time-dependent increase in fluorescence that varied for the different HPO, but maximum recovery was usually comparable for all the HPOs (not shown; Fig. 2A depicts only the levels attained after the addition of SIH). The normalized traces shown in Fig. 2A were also used for computation of rate constants of fluorescence recovery (see Fig. 4). Similar experiments were carried out with RSFs and DFOs that also vary in their PC. The traces of fluorescence recovery were aligned in decreasing order of chelator speed of action (Fig. 2B): m2pee, m2phe, m2ileu, m2leu, m2, N-methylanthranilic-DFO, and DFO. The relative speed of action followed the ranking order of PCs for the RSF series and the two DFOs.

**Iron chelation in K562 cells.** The effect of chelators on living cells was assessed in terms of chelator capacity to deplete the LIP and to extract LIP iron into the medium. The LIP was followed with *in situ* generated CA, which was loaded into cells via the AM form. A 5-min incubation with 125 nM CA-AM at 37° yielded ~5–10 $\mu$M intracellular CA, mostly in the cytosol (11, 12). Anti-CA antibody was added to ascertain that all the recorded fluorescence was intracellular and that CA leakage from cells was insignificant. After a stable signal was obtained after the addition of antibody, chelators were added to cells. As with resealed ghosts, the time-dependent increase in cell-associated fluorescence indicates the relative speed of chelator entry into cells and binding of LIP iron. All systems were normalized to the LIP level of cells, which is given by the difference between the initial fluorescence intensity and the maximum fluorescence attained after the addition of SIH (100 $\mu$M). The relative change in fluorescence intensity obtained after the addition of SIH was highly reproducible, despite the fact that it was ~5% of the total signal intensity. Fig. 3A depicts the fluorescence recovery as a function of the concentration of HPO102, a representative hydrophilic HPO. Although data could be fitted to an apparently linear plot (r = 0.9), as seen (*inset*), a linear dependence of cell iron chelation (given by the rate

**Fig. 2.** Dequenching of CA/iron complexes encapsulated in resealed ghosts by extracellularly added HPOs. CA-loaded ghosts (50 $\mu$M intracellular concentration) were pretreated with FAS until 70% of the total fluorescence signal or > 90% of the ghost-associated fluorescence signal was quenched (by penetration of FAS and intracellular quenching). A, CA/iron-laden ghosts were exposed to different HPOs (165, 41, 117, 20, and 40) at the time indicated (*arrows*), followed by 100 $\mu$M SIH (∗). B, CA/iron-laden ghosts were exposed to various RSFs (100 $\mu$M concentration), followed by 100 $\mu$M SIH (∗). Data are depicted as in Fig. 1. See Table 1 for chemical structures.

constant) on HPO102 concentration was attained only at concentrations of >30 $\mu$M (r = 0.98) (Fig. 3A, *inset*). This has to do with the fact that HPO/iron complexes have a >1:1 stoichiometry, probably closer to 3:1 (6), so a linear dependence is not expected at a relatively low concentration of the chelator. Therefore, a comparative study of HPO spanning a wide range of PCs was performed using various chelator concentrations. In Fig. 3B, we depict the profiles of fluorescence dequenching induced by various chelators at a 100 $\mu$M concentration. Similar profiles were obtained for different concentrations of chelators (not shown), which were used for estimation of the apparent rates of fluorescence recovery (Fig. 3B, *inset*), as given in the legend to Fig. 3B. The rates clearly indicate major differences in the capacity of HPOs for
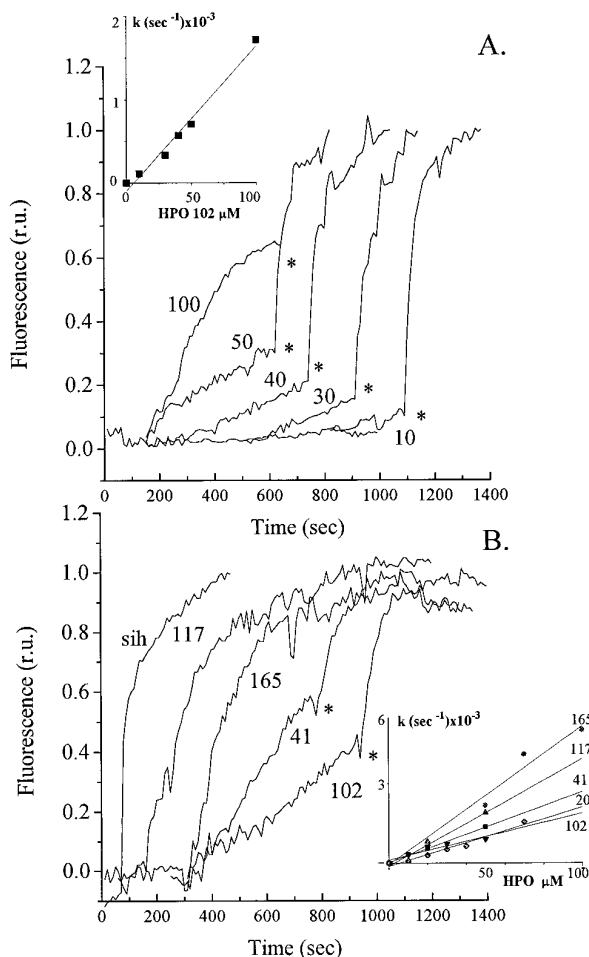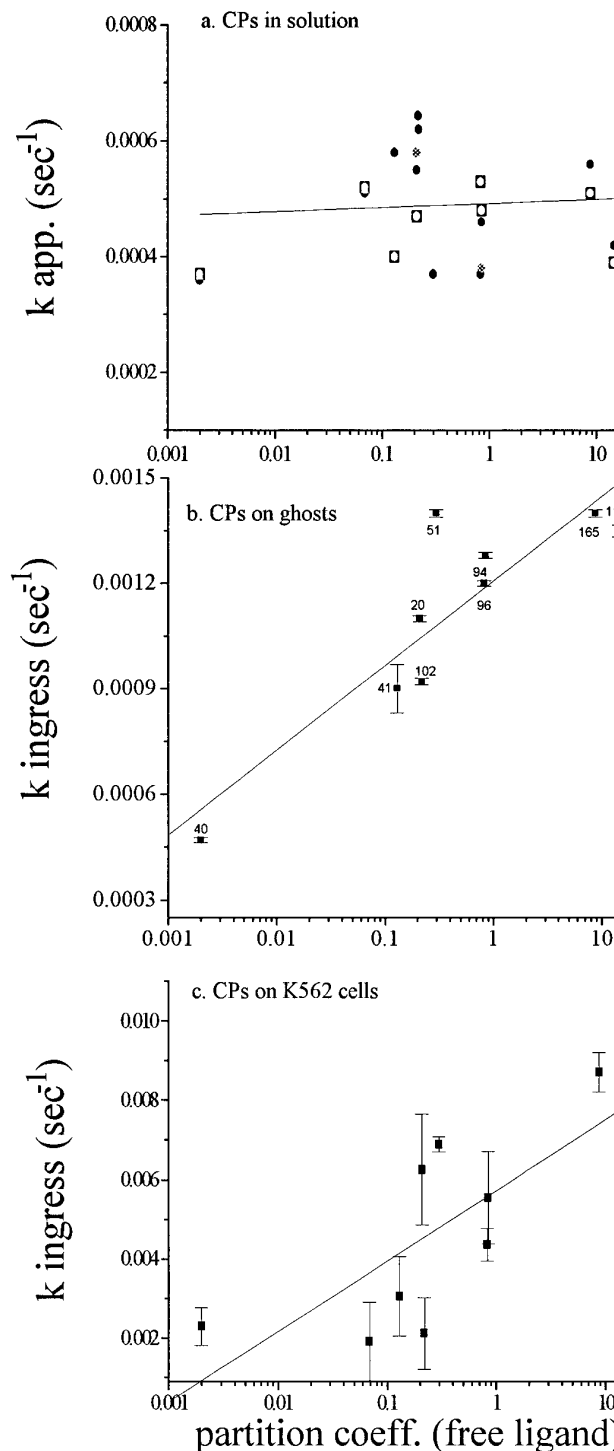
**Fig. 3.** Dequenching of CA/iron complexes in K562 cells by extracellularly added HPOs. CA-loaded K562 cells were treated with various concentrations of the HPO102 (A) or with different HPOs (117, 165, 41, and 102) added at a 100 $\mu$M final concentration (B). SIH (100 $\mu$M) was added at the point indicated (*) (A and B) to obtain maximum recoverable fluorescence. Data were normalized to the total increase in fluorescence attained by the addition of SIH. Scale shows relative fluorescence units (r.u.) against time (sec). Background fluorescence of CA-loaded cells represented 10% of the maximal fluorescence signal. *Inset*, concentration dependence of the initial rate of fluorescence dequenching ($k$ in sec$^{-1}$) obtained from the profiles shown in A for a representative compound of the HPO family (see Table 1 for chemical structures of HPOs). B, *inset*, same as A, *inset*, but for all of the HPOs tested. The linear regression lines for the various compounds gave the following slopes (first-order rates in $\mu$M/sec/10$^{-5}$, mean $\pm$ standard deviation): 6.0 $\pm$ 0.7 (HPO165) ($r$ = 0.99), 4.0 $\pm$ 0.6 (HPO117) ($r$ = 0.98), 3.0 $\pm$ 0.1 (HPO41) ($r$ = 0.99), 2.0 $\pm$ 0.4 (HPO20) ($r$ = 0.94), and 2.0 $\pm$ 0.2 (HPO102) ($r$ = 0.99).

intracellular chelation over the entire range of chelator concentrations. That capacity increased with the lipophilicity of the chelator.

The rate constant values shown in Fig. 3, A and B, as well as those corresponding to chelator action in solution and in resealed ghosts (data shown in Figs. 1 and 2), were compiled to correlate between the speed of HPO binding of iron and the PC of the HPO free ligand (Fig. 4, A–C). Although the PC of the free ligand hardly affected the rate constant of iron binding (Fig. 4A), it demonstrably affected the rate constant of chelator entry and binding of compartmentalized iron in membrane ghosts and K562 cells (Fig. 4, B and C). For these two membrane systems, the correlations were qualitatively



**Fig. 4.** Correlation between dequenching of CA/iron complex in solution (a), ghosts (b), and K562 cells (c) by extracellularly added HPOs and their PCs. The rate constant of dequenching ($k_{app}$ in sec$^{-1}$) in solution by HPOs (a), ingress of HPOs into ghosts ($k_{ingress}$ in sec$^{-1}$) (calculated from data shown in Fig. 2A) (b), or into K562 cells (calculated from data shown in Fig. 4) (c) are plotted against the PC of the free ligand of the HPO. a, No apparent correlation could be found. b (ghosts), slope was 2.4 $\pm$ 0.5 $\times$ 10$^{-4}$ sec$^{-1}$ ($r$ = 0.88). c (K562 cells), slope was 1.8 $\pm$ 0.5 $\times$ 10$^{-3}$ sec$^{-1}$ ($r$ = 0.80).

similar despite the fact that in resealed ghosts, the CA/iron concentration was relatively high and most of the CA-bound metal was iron(III), whereas in K562 cells, the chelatable

iron (or LIP) was markedly lower and was composed primarily of iron(II) (10). These findings suggest that the limiting step in fluorescence recovery, as determined by the calculated rate constant, is the permeation of the chelator across the respective membrane.

A similar approach using CA-loaded K562 cells was applied to the hydroxamate-based chelators. RSFs were used at a 30 μM concentration, based on their property of forming 1:1 complexes with iron rather than the 3:1 complexes formed by the HPOs (7). In Fig. 5A, we depict the fluorescence-recovery profiles induced by different concentrations of one of the most hydrophilic members of the RSF family, RSFm2. Similar studies were carried out with the lipophilic RSFm2phe (or simply RSFphe) (not shown). The profiles were used for obtaining the apparent first-order rate constants at different concentrations of chelators, which were plotted against each other in Fig. 5A (*inset*) for both chelators. The rate of fluorescence dequenching, which results from intracellular chelation, increased markedly with the lipophilicity of the RSF
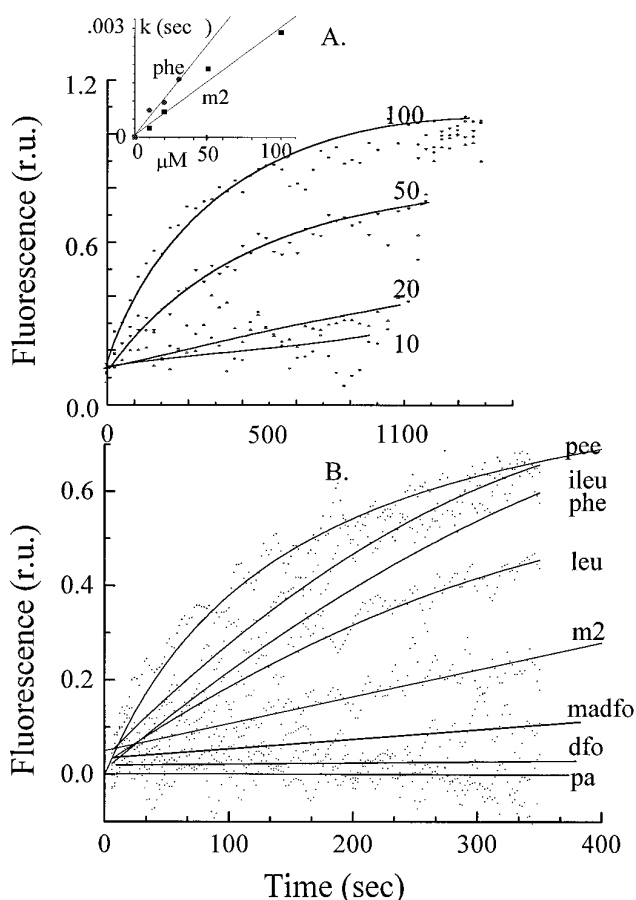


**Fig. 5.** Dequenching of CA/iron complex in K562 cells by extracellularly added RSFs . CA-loaded K562 cells were treated with (A) various concentrations of RSFm2 and (B) various RSFs (30 μM) or DFOs (200 μM). Data were normalized to the total increase in fluorescence attained by the addition of SIH. *Scale*, relative fluorescence units (r.u.) against time (sec). Background fluorescence of CA-loaded cells represented 10% of the maximal fluorescence signal. A, *Top*, concentration dependence of fluorescence recovery evoked by RSFm2. *Inset*, dependence of the apparent rate constant obtained from by RSFm2 (5A) and RSFphe (not shown) with the chelator concentration (for both RSFm2 and RSFphe). The calculated slopes (first-order rates, in $\mu M^{-1}$ $sec^{-1}$) were $3.0 \pm 0.2 \times 10^{-5}$ ($r = 0.98$) for RSFm2 and $7.0 \pm 0.6 \times 10^{-5}$ ($r = 0.98$) for RSFphe.

and linearly with the chelator concentration (Fig. 5, *inset*). This is also evident from Fig. 5B, in which various RSFs at the concentration of 30 μM and DFOs at a concentration of 100 μM were compared because at <50 μM, the two DFOs had no effect over a 2-hr period. The efficacy of RSFs clearly increased with the lipophilicity of the chelator although apparently to a relatively lesser extent than for the HPOs.

**Chelator-mediated cellular $^{55}$Fe release.** K562 cells loaded with $^{55}$Fe-Tf were incubated for 0–4 hr at 37° in the presence of chelators, and the amount of radioiron released into the medium was determined as a function of time. Fig. 6 depicts the egress of $^{55}$Fe from cells into medium in the presence of SIH, HPO117, a hydrophobic HPO, or DFO. The radioactivity appearing in the medium increased with time in the presence of SIH and HPO117 and reached a plateau within 2 hr. In contrast, DFO caused no significant release of $^{55}$Fe compared with control. We used the 30-min time point of $^{55}$Fe release for comparing the iron-extraction efficacy of the various classes of chelators. Values are given relative to egress induced by SIH so we could pool data obtained from different experiments with different cell preparations (Fig. 7, A and B).

The correlations between $^{55}$Fe extraction and the PC of the iron-chelator complex are given in Fig. 8, A and B. The HPOs could be divided into three distinct groups according to their PCs and iron-extraction efficacy: a hydrophilic group of low efficacy (HPO40, HPO20, HPO102, and HPO51), a lipophilic group with high efficacy (HPO117 and HPO165), and an intermediate group (HPO96, HPO94, and HPO41). A similar relationship was found for the RSF compounds. The relatively more hydrophilic m2 showed low extraction efficacy, whereas the more lipophilic ones were relatively more effective. It should be noted that the iron-extraction efficacy of
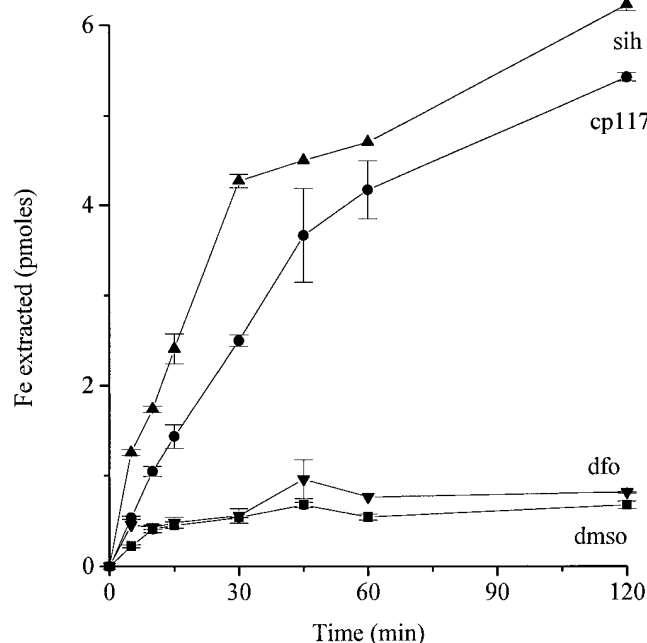


**Fig. 6.** Time-dependent $^{55}$Fe release from K562 cells into the medium by SIH, HPO117, and DFO. Tf-$^{55}$Fe-prelabeled K562 cells were incubated for 0–240 min at 37° in the presence or absence of HPO117, DFO (100 μM), and DMSO, and $^{55}$Fe release in the medium was measured. *Scale*, iron extracted (pmol) versus time (min). Values are mean ± standard deviation ($n = 5$).
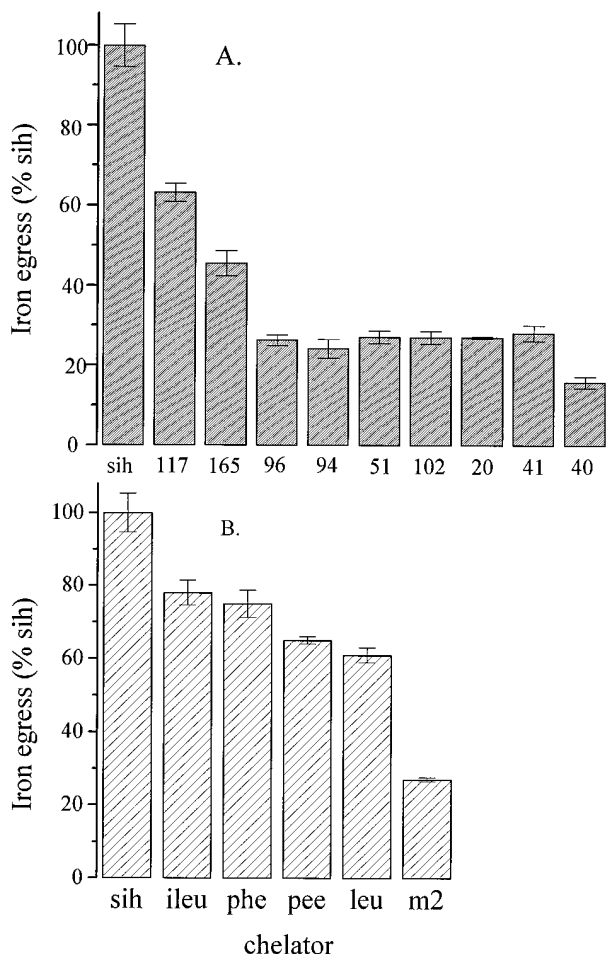
**Fig. 7.** $^{55}$Fe release from K562 cells by (A) HPOs and (B) RSFs in decreasing order of lipophilicity. TF-$^{55}$Fe-prelabeled K562 cells were exposed for 30 min to different (A) HPOs (100 $\mu$M) or (B) RSFs (100 $\mu$M), and $^{55}$Fe release in the medium was measured. *Scale*, $^{55}$Fe egress in percentage relative to that recovered by SIH. Values are mean $\pm$ standard deviation ($n = 6$). Lipophilicity values are given in the legend to Fig. 8

HPOs or RSFs that have potentially cleavable ester groups, such as HPO117 and HPO165 and RSFmePEE, correlated with their respective PC of the uncleaved complexes and not with those of the respective cleaved products, HPO40, HPO102, and RSFm2PA. Because the latter are poorly permeant as either free ligands or iron complexes, the results imply that the compounds were not intracellularly deesterified during the course of the experiments.[2]

**Cell toxicity of iron chelators.** To assess the toxic potential of the agents tested in this study, we measured their effects on DNA replication and total nucleic synthesis, as described for other chelators (9, 19). Hydroxyurea and DFO were taken as a test inhibitors (9, 19, 20). The assays were carried out after overnight incubation in the presence of a given drug concentration (continuous drug exposure) and after washing of the cells and resuspension of them in drug-free medium (drug exposure and removal = residual effect). We used incorporation of $^3$H-labeled thymidine and $^3$H-la-
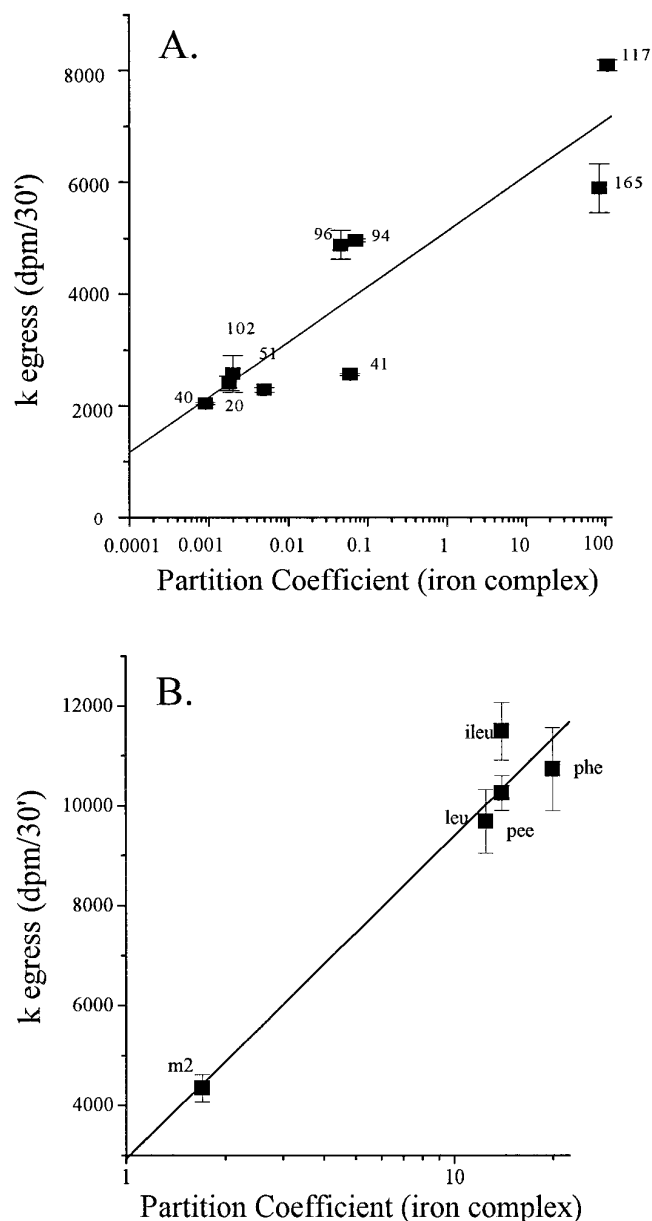


**Fig. 8.** The relationship between the lipophilicity of (A) HPOs, (B) RSFs, and $^{55}$Fe release from K562 cells. The rates of egress ($k$ in dpm/30′) of different (A) HPOs and (B) RSFs were plotted against the PCs of the respective iron complex. Linear relations ($r \geq 0.94$) were observed for both HPOs and RSFs. Values were mean $\pm$ standard deviation ($n = 6$). See Table 1 for chemical structures.

beled hypoxanthine (not shown) into macromolecules as a measure of the cell synthetic capacity. As described in our earlier studies with other chelators (9, 19, 20), DFO and hydroxyurea had significant inhibitory effects on DNA synthesis when present during the labeling period. Under these conditions, none of the HPOs had significant effects on DNA synthesis when used at $\leq$50 $\mu$M (Table 2) or on total nucleic acid synthesis when used at $\leq$100 $\mu$M concentrations (not shown). Moreover, only minor residual inhibitions were found after removal of the drugs, and in some cases (e.g., hydroxyurea and some HPOs), removal of the drug gave an apparent stimulation. This rebound effect found with nucleic acid synthesis has been noticed before with similar agents (19, 20) and has been attributed to the synchronizing effect of

---

[2] It remains to be determined whether the esterified HPO117 is cleaved inside K562 cells to its free acid, HPO102. In rats, the metabolite HPO102 was indeed detected in the bile 10 min after intravenous administration of HPO117 (17).

TABLE 2
**Effect of HPOs on DNA synthesis under continuous exposure to drug and after drug removal (residual)**

K562 cells exposed for 16 hr (overnight) to the indicated concentrations of HPO, DFO, and hydroxyurea were assessed for DNA synthesis as described in Materials and Methods. Data are given as mean $\pm$ standard error ($n = 4$) of $^3$H-thymidine incorporation into macromolecular material relative to the respective control (100%), which contained the same amount of DMSO but no drug. The respective incorporations of labeled material for the controls were 23,032 $\pm$ 3,950 dpm/well (continuous exposure) and 31,590 $\pm$ 2,100 dpm/well (residual).

| Drug ($\mu$M) | Drug effects on nucleic acid synthesis | |
| --- | --- | --- |
| | Continuous exposure | Residual |
| None | 100 $\pm$ 10 | 100 $\pm$ 6 |
| Hydroxyurea | 60 $\pm$ 2[a] | 126 $\pm$ 7 |
| DFO (100) | 21 $\pm$ 7[a] | 104 $\pm$ 4 |
| CP94 (10) | 126 $\pm$ 22 | 84 $\pm$ 12 |
| CP94 (50) | 95 $\pm$ 11 | 73 $\pm$ 16 |
| CP102 (10) | 115 $\pm$ 12 | 101 $\pm$ 13 |
| CP102 (50) | 106 $\pm$ 7 | 94 $\pm$ 6 |
| CP20 (10) | 97 $\pm$ 4 | 124 $\pm$ 6 |
| CP20 (50) | 107 $\pm$ 3 | 112 $\pm$ 9 |
| CP40 (10) | 113 $\pm$ 4 | 140 $\pm$ 9 |
| CP40 (50) | 92 $\pm$ 4 | 97 $\pm$ 5 |
| CP41 (10) | 87 $\pm$ 7 | 119 $\pm$ 9 |
| CP41 (50) | 111 $\pm$ 16 | 137 $\pm$ 13 |
| CP165 (10) | 122 $\pm$ 10 | 145 $\pm$ 25 |
| CP165 (50) | 106 $\pm$ 3 | 144 $\pm$ 25 |

some agents that arrest cells at particular stages of the cell cycle.

## Discussion

The assessment of chelator efficiency in scavenging intracellular metals is of crucial importance in the design of tools for the treatment of iron-overload diseases (16). Iron chelators are used in these settings to reduce the excessive body stores of the element and thereby prevent complications. To develop new iron chelators, it is also important to understand which of the physicochemical properties are of importance in determining the speed at that chelators access cell LIPs and the speed and extent of net iron mobilization from different cells. In this study, we focused on K562 erythroleukemia cells because these cells have been extensively studied in terms of their iron-regulatory properties. In the conditions used in the current study, none of the HPOs (Table 2), DFOs (9, 19) or RSFs (9) had any residual effect on cell proliferation. This study is being extended to liver and cardiac cells, which are of more clinical relevance to iron overload.[3]

The combined fluorescence and radioactivity assays presented in this study provide complementary means for comparing the efficiency of iron scavenging in both a membrane model system and living mammalian cells. The continuous monitoring of iron scavenging by fluorescence was based on the application of the metallosensitive probe CA (11, 12), which was adapted in this study for assessing iron chelation efficiency in solution, in ghosts as a simple membrane model system, and in K562 cells as a model for cells growing in suspension. This method provided on-line information about the speed of chelator permeation across membranes and a measure for chelation of iron associated with LIP (11, 12). In resealed ghosts, most of the iron bound to CA is in the oxidized iron(III) form and is virtually inaccessible to a non-
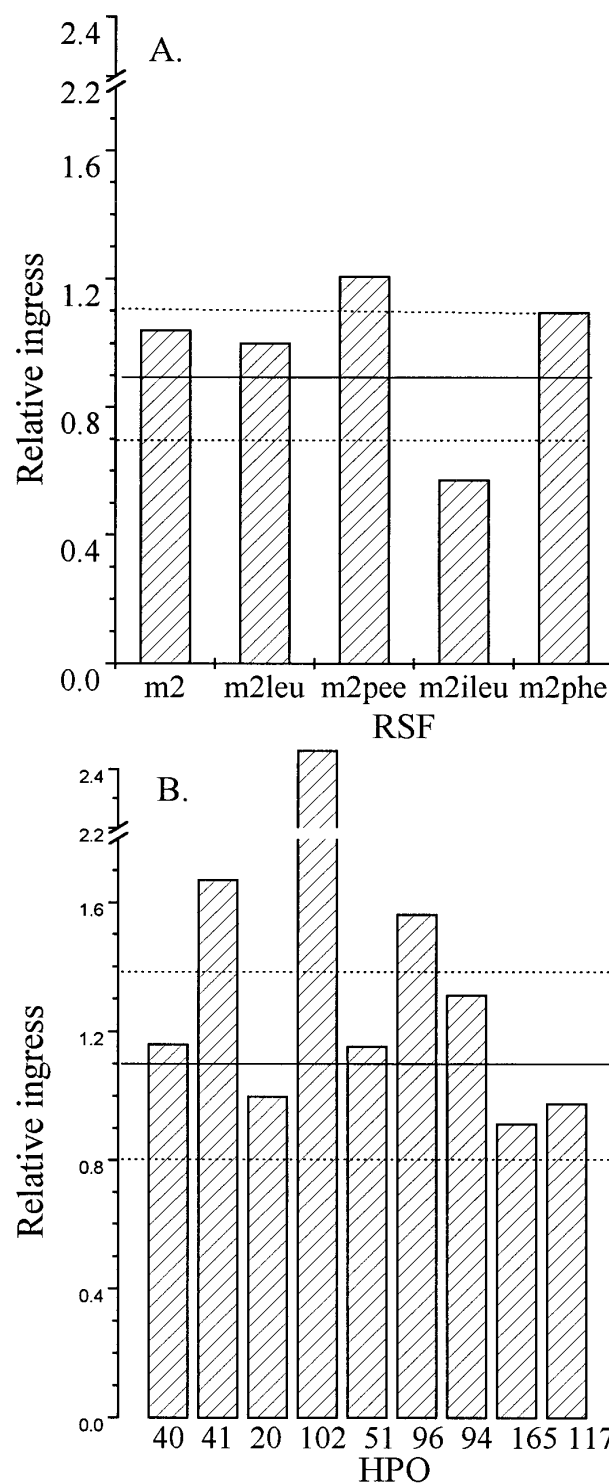
**Fig. 9.** The relationship between (A) RSFs and (B) HPO rates of ingress in ghosts and K562 cells. The rates of ingress of the various RSFs and HPOs into ghosts divided by the respective rates of ingress into K562 cells are given as relative ingress (for RSFs, the values were normalized to that of RSFm2leu, and for HPOs, the values were normalized to that of HPO20). The order of bars on the *x*-axis is from the chelator with (*left*) lowest to (*right*) highest PC. *Horizontal lines*, mean value of relative ingress (*full line*) $\pm$ standard error (*broken lines*) $\pm$ standard deviation.

permeating chelator such as DFO. This provides a highly sensitive and convenient means for comparative assessments of chelator capacity for scavenging iron from a simple mem-

brane-enclosed compartment. In K562 cells, the chelatable form of iron identified with the LIP is probably cytosolic iron(II) (11), and only a fraction of that iron is apparently bound to CA. However, despite the fact that chelator-induced recovery of fluorescence represents only a small percent of the total fluorescence signal (10), the method is also highly sensitive and reproducible for a comparative assessment of chelator action on living cells. It provides a reliable measure of how fast chelators cross biological membranes and bind iron in the accessible cellular pools (i.e., LIP).

As summarized in Fig. 4, for most members of the three families of chelators, the intracellular scavenging of iron was determined primarily by the lipophilicity of the chelator. Although such a property could be anticipated on physicochemical grounds and on the basis of previous studies (1, 2, 7), this is the first direct demonstration of a chelation process that is visualized continuously, kinetically, and spatially that takes place exclusively within the cell. The results clearly highlight the simplicity, versatility, and informative nature of the new methodology applied to two different biological systems (12). Both systems provided equivalent information regarding accessibility of internal iron pools to extracellularly added chelators as shown in Fig. 9. With the exception of HPO102 and RSFm2ileu, the relative efficacies of the chelators were demonstrably comparable in ghosts and K562 cells. The relatively higher efficacy of HPO102 in the model membrane system of ghosts versus K562 cells, or vice versa for RSFi leu, might represent a differential capacity for assessment of LIP in K562 cells, as apparent from Fig. 4c. However, these properties must be further evaluated. We have found that for comparative purposes, HPOs had to be used at relatively high concentrations ($>50$ $\mu$M) inasmuch as these agents form high stoichiometry (3:1) chelator/iron complexes, whereas the tris hydroxamate RSFs could be used at relatively lower concentrations, due primarily to their 1:1 binding stoichiometry. For the DFOs, higher concentrations were required to obtain dequenching profiles due to their poor permeation or access to intracellular iron pools.

The radioactive assay, on the other hand, provided the complementary step in the assessment of iron mobilization (i.e., the transfer of iron from cells into medium). This is the method most commonly used for assessing chelator extraction efficiency in cells, primarily after loading with labeled non-Tf-bound iron (7). We preferred the Tf-mediated route of iron loading to circumvent high background levels that unavoidably result from chelatable non-Tf-bound iron adsorption to cell and solid surfaces. As with the fluorescent method, the iron mobilization capacity was dictated by the PC of the chelator as free ligand or, better, as iron complex (Figs. 4 and 8). For RSFs and DFOs, which form 1:1 complexes with iron(III) without changing their overall net charge, the values of PCs are similar for the free and complexed ligand, so the permeation properties of the free and complexed chelators are expected to differ only slightly, as they indeed do (10). For HPOs, however, due to their 3:1 binding stoichiometry of iron(III) and retention of the electroneutral character, the lipophilicity increases after iron complexation with the lipophilic HPOs (PC $>$ 1) and decreases for the relatively hydrophilic HPOs (PC $<$ 1) (7). This property, as well as the relative size of the molecules, are likely to affect permeation of the free- versus the iron-complexed forms of the chelators. The efficacy of iron mobilization is a complex phenomenon that involves several counteracting factors. For HPOs, it is probably determined by the form of the chelator that has the lowest PC, and therefore the lowest permeation capacity across membranes. This differential permeation is of paramount importance not only for iron mobilization *per se* but also for cell survival, since an increased residence time of an iron/chelator complex in the cell might also expose it to the toxic action of iron complexed to agents such as HPOs (16). Moreover, chelators might undergo metabolic conversions, as often is the case with HPOs, particularly in hepatic cells (7). On the other hand, increased residence time of the free chelator might also increase the iron-extraction capacity by driving cells to release iron from stores or pools less labile than LIP. Empirically, it has been found that HPOs of intermediate PCs (0.2–1.0) apparently offer the best compromise between the above factors and have thus far been found to be the optimal orally active HPOs (13). The same is apparently applicable to SIH, which in the present study was the fastest acting of all the tested chelators, despite the relatively low lipophilicity (PC = 0.35) of the free ligand and of the iron complex (PC = 0.1; binding stoichiometry, 2:1) (7).

Based on the experimental record of DFO and other chelators, including HPOs, it is clear that iron extraction from organisms or cell model systems (18) is comparable for these two classes of agents. This was also found to be the case for those agents, including RSFs, when given to cells on a long term basis (3–24 hr) (19).[3] However, this apparently was not the case in the short term ($<$4 hr) because, as shown in this work, RSFs and HPOs were markedly superior to DFO when used in comparable or even less favorable conditions in K562 cells. In fact, for agents of comparable PCs, RSFs slightly outperformed HPOs in extracting iron from cells (Fig. 7). DFO was used at $\leq$200 $\mu$M, HPOs were used at $\leq$100 $\mu$M, and RSFs were used at 30 $\mu$M [to compensate for the 3:1 coordination ratio of HPO/iron complexes but not for the $10^{10}$-fold higher binding affinity of HPO for iron(III)]. Thus, the assays used in this work provide measures for the speed of action and efficacy of given series of structural congeners of a chelator as cell iron scavengers and mobilizing agents. These properties are correlated with and therefore largely influenced by the PC of the chelator when assessed on a short term basis. However, as observed with DFO in long term exposures, additional factors other than PC or even iron-binding affinity would seem to be compensatory and even dominant in determining the biological performance of a given chelator. This includes also possible toxic effects that are not observed in *in vitro* tests, such as those shown in this work (Table 2) and in previous studies (9, 19, 20). Thus, the relevance of the current study for clinical applications of iron chelators awaits further studies in cell and animal models of iron overload and of drug toxicity and pharmacokinetics associated with the mode of drug delivery.

### References

1. Hershko, C., and D. J. Weatherall. Iron-chelating therapy. *Crit. Rev. Clin. Lab. Sci.* **26:**303–345 (1988).
2. Hershko, C. Control of disease by selective iron depletion: a novel therapeutic strategy utilizing iron chelators, in *Bailliere's Clinical Haematology: Clinical Disorders of Iron Metabolism* (C. Hershko, ed.). Bailliere Tindall, London, 965–1000 (1994).
3. Nathan, D. G., and Piomelli S. Introduction: oral iron chelators. *Semin. Haematol.* **27:**83–85 (1990).
4. Hershko, C., A. Pinson, and G. Link. Iron chelation. *Blood Rev.* **4:**1–8 (1990).

5. Brittenham, G. M. Development of iron chelating agents for clinical use. *Blood* **80:**569–574 (1992).
6. Hider, R. C., and S. Singh. Iron chelating agents with clinical potential. *Proc. R. Soc. Edinb. Sect. B (Biol.)* **99:**137–168 (1992).
7. Porter, J. B., M. Gyparaky, L. C. Burke, E. R. Huehns, P. Sarpong, V. Saez, and R. C. Hider. Iron mobilization from hepatocyte monolayer cultures by chelators: the importance of membrane permeability and iron-binding constant. *Blood* **72:**1497–1503 (1988).
8. Porter, J. B., R. C. Hider, and E. R. Heuhns. Update on the hydropyridone oral iron-chelating agents. *Semin. Hematol.* **27:**95–100 (1990).
9. Shanzer, A., J. Libman, H. Glickstein, S. D. Lytton, and Z. I. Cabantchik. Reversed siderophores act as antimalarial agent. *Proc. Natl. Acad. Sci. USA* **88:**6585–6589 (1991).
10. Loyevsky, M., J. Lytton, B. Mester, J. Libman, A. Shanzer, and Z. I. Cabantchik. The antimalarial action of desferal involves a direct access route to erythrocytic (*P falciparum*) parasites. *J. Clin. Invest.* **91:**218–224 (1993).
11. Breuer, W., S. Epsztejn, and Z. I. Cabantchik. Iron acquired from transferrin by K562 cells is delivered into a cytoplasmic pool of chelatable iron(II). *J. Biol. Chem.* **270:**24209–24215 (1995).
12. Cabantchik, Z. I., H. Glickstein, P. Milgram, and W. Breuer. A fluorescence assay for assessing chelation of intracellular iron in a membrane model system and in mammalian cells. *Anal. Biochem.* **233:**221–227 (1996).
13. Dobbin, P. S., R. C. Hider, A. D. Hall, P. D. Taylor, P. Sarpong, J. B. Porter, and G. Xiao. Synthesis, physicochemical properties, and biological evaluation of N-substituted 2-alkyl-3-hydroxy-4 (1H)-pyridinones: orally active iron chelators with clinical potential. *J. Med. Chem.* **36:**2448–2458 (1993).
13a. Tsafack, J., J. Golenser, J. Libman, A. Shanzer, and Z. I. Cabantchik.

Mode of action of iron(III) chelators as antimalarials. III. Overadditive effects in the combined action of hydroxamate-based agents on *in vitro* growth of *Plasmodium falciparum. Mol. Pharmacol.* **47:**403–409 (1995).
14. Ponka, P., R. W. Grady, A. Wilczynska, and H. M. Schulman. The effect of various chelating agents on the mobilization of iron from reticulocytes in the presence and absence of pyridoxal isonicotinoyl hydrazone. *Biochim. Biophys. Acta* **802:**477–489 (1984).
15. Dayan J, J. Libman, Y. Agi, and A. Shanzer. Chiral siderophores analogs: ferrichrome I. *Inorg. Chem.* **32:**1467–1475. (1993).
16. Porter, J. B., E. R. Huehns, and R. C. Hider. The development of iron chelating drugs. *Bailliere's Clin. Haematol.* **2:**257–292 (1989).
17. Zanninelli, G., J. B. Porter, O. Loreal, G. Lescoat, B. Cosson, R. Verna, and P. Brissot. Biliary excretion of plasma NTBI in the rat is enhanced by the novel hydroxypyrid-4-one oral chelators. *Hepatology* **22:** 309A (1995).
18. Kontoghiorghes, G., and A. V. Hoffbrand. Orally active α-ketohydroxy-pyridine iron chelators intended for clinical use: *in vivo* studies in rabbit. *Br. J. Haematol.* **62:**607–613. (1986).
19. Glickstein, H., W. Breuer, M. Loyevsky, A. M. Konijn, J. Libman, A. Shanzer, and Z. I. Cabantchik. Differential cytotoxicity of iron chelators on malaria infected cells versus mammalian cells. *Blood* **87:**4871–4878 (1996).
20. Lytton, S. J., B. Mester, H. Glickstein, I. Dayan, J. Libman, A. Shanzer, and Z. I. Cabantchik. Mode of action of iron(III) chelators as antimalaria agents II: evidence for differential effects on parasite-dependent nucleic acid synthesis. *Blood* **84:**910–915 (1994).

**Send reprint requests to:** Dr. Z. Ioav Cabantchik, Department of Biological Chemistry, Institute of Life Sciences, Hebrew University Jerusalem, Jerusalem, Israel 91904. E-mail: ioav@cc.huji.ac.il